Optical determination of temperature and species concentration for homogeneous turbulent gas medium

Tao Ren, Michael F. Modest*

School of Engineering, University of California, Merced, California, USA

Abstract

In this study, we present an inverse calculation model to reconstruct time-averaged temperature, species concentration and their root mean square (rms) values from optical synthetic measurements for a homogeneous turbulent gaseous medium. The model is based on line-of-sight spectral transmissivity synthetic measurements, and time-averaged transmissivities and their rms values are successfully related to time-averaged temperatures, species concentrations and their rms values by considering interaction between turbulence and radiation (TRI). The turbulence length scale is also retrieved simultaneously with the turbulent scalars. In order to validate the model, a stochastic approach is used to generate synthetic turbulent fields (fluctuations of temperature and species concentration), and measured spectra are synthesized through calculations from HITEMP 2010 for different spectral bands of CO_2, H_2O and CO.

Keywords: turbulence, radiation, temperature, concentration, transmissivity

Nomenclature

B	gradient vector
f	nonlinear function
F	objective function
g	nonlinear function
H	Hessian matrix
L	length of the gas cell, cm
P	total pressure, bar
s	length along path, cm
t	total time interval, s
t_e	turbulence integral time scale, s
T	temperature, K
u	turbulent scalar
U	standard deviation for the turbulent scalar
x	concentration by volume

Greek Symbols

β	percentage of turbulence fluctuation
η	wavenumber, cm^{-1}
θ	turbulence effects from spatial correction
κ	absorption coefficient, cm^{-1}
τ	transmissivity
χ	turbulence optical thickness

*Corresponding author. Tel.: +1 209 228 4113.
Email address: mmodest@ucmerced.edu (Michael F. Modest)

Γ pixel response function (PRF)
Λ turbulence integral length scale, cm

1. Introduction

Advanced optical diagnostics and multi-scale simulation tools will play a central role in the development of next-generation clean and efficient combustion systems, as well as in upcoming high-temperature alternative energy applications. High-fidelity experimental diagnostics will be required to validate advanced numerical models, and both are needed to guide the move toward nonpetroleum-derived fuels, high operating temperature and pressure, etc. Combustion diagnostics have reached high levels of refinement, but it remains difficult to make quantitatively accurate nonintrusive measurements of temperature and species concentrations in realistic combustion environments. Measurements of temperature and species concentrations in combustion fields are usually not directly accessible and have to be inferred from experimentally measurable quantities by solving an inverse problem. Griffith et al. [1, 2] were the first to recognize that measurements of the transmissivity or emissivity of rotational spectral lines of a gas can reveal its temperature. Work has been done to extract temperature and species concentration for laminar combustion system [3–12] based on optical measurements of transmission or emission. For a turbulent system, it has long been recognized that the nonlinear interaction between turbulence and radiation (TRI) has profound effects on the heat transfer of turbulent combustion systems [13–17], leading to sharply increased radiative heat loads to the adjacent walls and surroundings. The radiative signal from combustion gases is influenced by nonlinear interaction with turbulence. In the presence of TRI, temperature and concentration must be deduced using knowledge of turbulence structures or employing TRI models.

Experimental investigations by Faeth and Gore [18–31] and probability density function (PDF) based calculations [32–36] have shown that TRI always increases the heat loss from a flame, and this additional heat loss can reach 60% of the total and more, leading to a reduction in the local gas temperature of 200 $^{\circ}$C or more. Therefore, the radiative signal hitting a detector is influenced by the nonlinear interaction with turbulence. The TRI effects, although acknowledged and qualitatively understood over the last three decades or so, are extremely difficult to model. Most work in TRI has been devoted to the study of turbulence on total radiative heat transfer emitted by a hot medium. A rather different challenge is accurate modeling of the correlation between local instantaneous radiation intensity along the optical path and local absorption coefficients [37]. Most works have neglect this correlation based on the suggestion and arguments given by Kabashnikov and Myasnikova [38] that, if the mean free path for radiation is much larger than the turbulence length scale, then the local intensity is governed by fluctuations far away, and thus should be only weakly correlated with local absorption coefficient fluctuations. This assumption appears to be valid over most of the gas spectrum for small-scale, lower-sooting flames and is known as the optically thin fluctuation assumption (OTFA), but questionable for very strong spectral lines. Ko et al. [39] developed a spectral remote sensing method to retrieve mean temperature and concentration from spectral turbulent intensities using the CO_2 4.3 μm band by applying the OTFA. For their proposed method, it is claimed that the coupled temperature/concentration fluctuation amplitudes and mean values can be successfully inverted from optically measured intensity spectra. However, only retrieved mean temperature/concentration profiles along the path were presented and not much detail was given for the inverse method. Unlike modeling TRI on spectral intensity, TRI on transmissivity can be accurately modeled by assuming the pdf shape of the absorption coefficient. An early study by Foster [40] showed that calculation of the mean transmissivity from a turbulent flame must take turbulent fluctuations into account. Coelho [37] showed that, in the presence of turbulent fluctuations, the turbulent fluctuation of the absorption coefficient increases the transmissivity of the medium if the pdf of the absorption coefficient is Gaussian and his observation is in agreement with the theoretical findings of Foster [40].

In the present study, by assuming the pdf shape of temperature and species concentration fluctuations, time-averaged transmissivity and its rms spectrum are successfully related to the time-averaged and rms values of temperature and species concentration; this is the so-called forward calculation. Once these relationships are established, time-averaged and rms values of temperature and species concentration and turbulence scales can be retrieved from time-averaged transmissivity and its rms spectrum; this is the so-called inverse calculation.

The absorption coefficients, which are required to calculate transmissivity and its rms spectrum, are calculated from HITEMP 2010, the high-temperature molecular spectroscopic database [41]. The database was extensively tested against measured FTIR spectra of CO_2 [42–44] and H_2O [45, 46]. Good agreement between measured and calculated spectra was found. For the present work, synthetic turbulent fields for temperature and species concentration fluctuations are generated by a stochastic approach. Instantaneous transmissivity spectra are generated along a line-of-sight for different spectral bands of CO_2, H_2O and CO. Synthetic time-averaged transmissivities and their rms spectra are calculated by conducting a stochastic analysis on these instantaneous transmissivity spectra and are used as input data to retrieve time-averaged and rms values of temperature, species concentration and turbulence length scale.

2. Instantaneous turbulence fields

A stochastic approach developed by Kritzstein and Soufiani [47] is adopted here, in which instantaneous temperature and species concentration fields are generated by Fourier transforming an assumed space-time correlation function. Without specifying the entire geometry of the system, turbulent scalar fields are created along a line-of-sight over a gas column of length L and for the time interval $0 \leqslant t \leqslant t_0$. The scalar fields are assumed to be stationary, homogeneous stochastic process, with a Gaussian probability density function. They are determined from these assumptions and the following properties:

$$\langle u'(s,t)\rangle = 0 \tag{1}$$

$$\langle u(s,t)u(s+r,t+\tau)\rangle = U^2 C(r,\tau) \tag{2}$$

where a prime denotes a fluctuation about the local mean value and angle brackets denote time-averaged quantities. The generated scalar field $u(s,t)$ is assumed to have a zero mean, a standard deviation $U = 1$ and to statistically satisfy a space-time correlation function:

$$C(r,\tau) = C_s(r)C_t(\tau) \tag{3}$$

where $C_s(r) = e^{-r/\Lambda}$ is the two-point/one-time correlation function and $C_t(\tau) = e^{-\tau/t_e}$ is the one-point/two-time correlation function, and Λ and t_e are the turbulence integral length scale and time scale, respectively. Kritzstein and Soufiani [47] studied the TRI effect for different forms of spatial correlation function and concluded that the contribution of turbulence on radiation is not very sensitive to the shape of the spatial correlation function. Therefore, in this study we only use exponential decay functions for both spatial and temporal correlation functions. Temperature and species concentration fields are generated by

$$T(s,t) = T_0\left[1 + \beta_T u'_T(s,t)\right] \tag{4a}$$

$$x(s,t) = x_0\left[1 + \beta_x u'_x(s,t)\right] \tag{4b}$$

where β_T and β_x represent the percentage of temperature and species concentration fluctuations around mean temperature and concentration T_0 and x_0, respectively. $u'_T(s,t)$ and $u'_x(s,t)$ are turbulent fluctuations used to generate temperature and species concentration fields satisfying properties as in Eqs. (1) and (2). The reader is referred to [47, 48] for more details on the approach of numerically generating the turbulent scalar fields.

Once temperature and species concentration fields along a line-of-sight are obtained, instantaneous spectral transmissvities $\tau_\eta(t)$ can be calculated as

$$\tau_\eta(t) = e^{-\int_0^L \kappa_\eta(T,x)\mathrm{d}s} \tag{5}$$

where $\kappa_\eta(T,x)$ is the spectral absorption coefficient calculated from the HITEMP 2010 line-by-line (LBL) database. Since transmissivity spectra can only be measured at a finite resolution by a spectrometer, the LBL spectral transmissvities of Eq. (5) have to be convolved with an pixel response function (PRF) to mimic the resolution of a spectrometer. After the transmissivity spectra are convolved with the PRF $\Gamma(\eta)$, they become,

$$\tau_{\eta c}(t) = \int_0^\infty \tau_\eta(t)\Gamma(\eta - \eta_1)\mathrm{d}\eta_1 \tag{6}$$

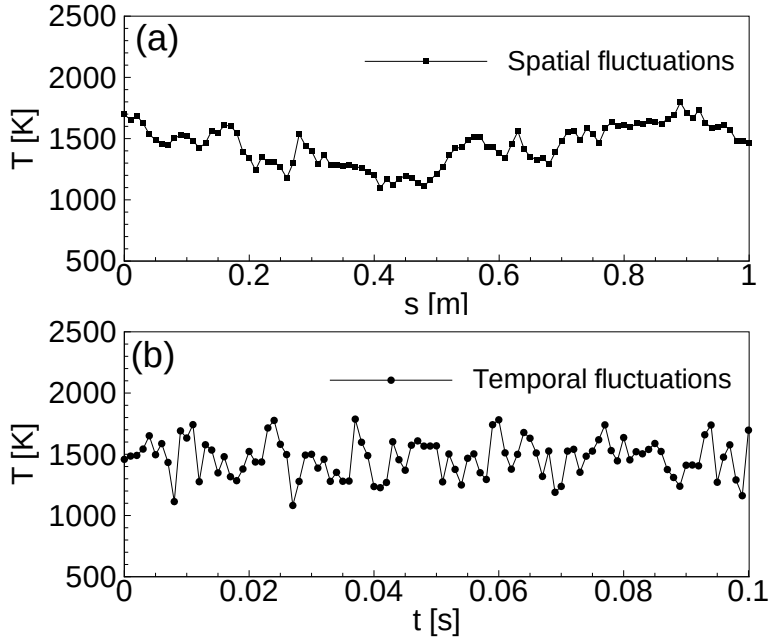

Figure 1: Demonstration of (a): spatial temperature fluctuations at an arbitrary time and (b) temporal temperature fluctuations at an arbitrary location

The PRF $\Gamma(\eta)$ we used here is

$$\Gamma(\eta) = \frac{0.666}{Res}\mathrm{sinc}^2\left(\frac{0.666\pi}{Res}\eta\right) \tag{7}$$

where *Res* is the nominal resolution of the PRF. In the present study, LBL spectral transmissivity are convolved with an PRF with nominal resolution of 4 cm^{-1} to create instantaneous medium-resolution transmissivity spectra based on the generated turbulent scalars filed.

Instantaneous scalar fields were created with an integral length scale of Λ for a gas medium of length L and with an integral time scale of t_e for a total time interval of t. Time-averaged transmissivity $\langle\tau_c(\eta)\rangle$ and its variance $\left\langle\tau_c'(\eta)^2\right\rangle$ can be obtained by conducting a stochastic analysis over the instantaneous transmissivity of Eq. (6). These values are used as input data to retrieve time-averaged temperature $\langle T\rangle$, concentration $\langle x\rangle$ and their variances $\left\langle T'^2\right\rangle$, $\left\langle x'^2\right\rangle$ and $\langle T'x'\rangle$. The retrieved statistical data will be compared with the the ones directly calculated from the created turbulent scalar fields. Assuming that the mean temperature T_0 of the gas medium is 1500 K and mean species concentration x_0 is 0.1, instantaneous turbulence fields were generated. Temperature and species concentration have 10% fluctuations around the mean values. These values were chosen to represent physical conditions, which are typical of the far-field self-preserving region of a turbulent reacting jet, downstream of the location where combustion has taken place [51]. Temperature and species concentration fields are created for 100 spatial points along the gas column of 1 m and for 1000 time realizations in 1 s. The integral length and time scales are 0.1 m (Λ=0.1 L) and 0.1ms, respectively, which makes a spatially correlated and temporally independent turbulence field. Figure 1 shows representative spatial temperature fluctuations at an arbitrary time and temporal temperature fluctuations at an arbitrary location for the created turbulent temperature field. Figure 2 shows typical correlation functions computed from the stochastic scalars fields as described above, averaged over 1000 time realizations for all the spatial points (error bars represent standard deviation of computed correlation functions for all the spatial locations), which is compared with the theoretical spatial correlation function $C_s(r) = e^{-r/\Lambda}$.

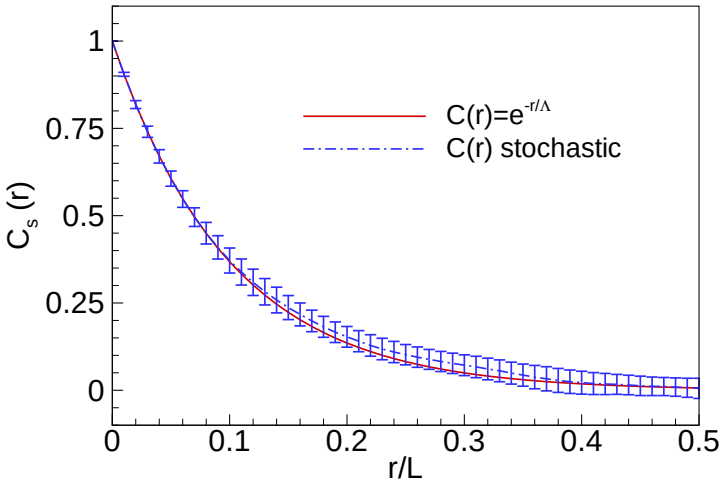

Figure 2: Comparison of theoretical spatial correlation function $C_s(r) = e^{-r/\Lambda}$ with the correlation function calculated from the created turbulence fields

3. Forward calculation

In order to retrieved mean scalars and their rms values from optically measured transmissivity and its rms spectra, it is important to have an accurate forward calculation model that can relate the mean and rms transmissvities to the mean and rms values of temperature and concentration. It is assumed that the time-averaged transmissivity and its variance can be measured in a finite resolution. Also, it is assumed transmissivities vary temporally and the fluctuation has zero mean. The forward calculation model is using time-averaged temperature $\langle T \rangle$, concentration $\langle x \rangle$ and their variances $\left\langle T'^2 \right\rangle$, $\left\langle x'^2 \right\rangle$ and $\langle T'x' \rangle$ to predict the measured time-averaged transmissivity $\langle \tau_c(\eta) \rangle$ and its variance $\left\langle \tau_c'(\eta)^2 \right\rangle$, which involves several levels of calculation.

3.1. From temperature and concentration to LBL absorption coefficient

It is known that absorption coefficient κ_η tends to be relatively linear in T and x, and it is reasonable to assume that

$$\kappa_\eta(T,x) \approx \kappa_\eta\left(\langle T \rangle, \langle x \rangle\right) + \frac{\partial \kappa_\eta(\langle T \rangle, \langle x \rangle)}{\partial T} T' + \frac{\partial \kappa_\eta(\langle T \rangle, \langle x \rangle)}{\partial x} x' \tag{8}$$

where temperature and concentration fluctuations T' and x' are assumed to be Gaussian random variables with zero mean. Taking the average of Eq. (8) leads to

$$\left\langle \kappa_\eta \right\rangle \approx \kappa_\eta(\langle T \rangle, \langle x \rangle) \tag{9}$$

This basically means the time-averaged absorption coefficient can be calculated from time-averaged temperature and species concentration. The variance of the absorption coefficient is defined as the mean-square fluctuation of the absorption coefficient. Combining Eqs. (8) and (9), the variance of κ_η can be deduced as

$$\begin{aligned} \left\langle \kappa_\eta'^2 \right\rangle &= \left\langle \left(\kappa_\eta - \left\langle \kappa_\eta \right\rangle\right)^2 \right\rangle \approx \left\langle \left[\frac{\partial \kappa_\eta(\langle T \rangle, \langle x \rangle)}{\partial T} T' + \frac{\partial \kappa_\eta(\langle T \rangle, \langle x \rangle)}{\partial x} x' \right]^2 \right\rangle \\ &= \left[\frac{\partial \kappa_\eta(\langle T \rangle, \langle x \rangle)}{\partial T} \right]^2 \left\langle T'^2 \right\rangle + \left[\frac{\partial \kappa_\eta(\langle T \rangle, \langle x \rangle)}{\partial x} \right]^2 \left\langle x'^2 \right\rangle + 2 \frac{\partial \kappa_\eta(\langle T \rangle, \langle x \rangle)}{\partial T} \frac{\partial \kappa_\eta(\langle T \rangle, \langle x \rangle)}{\partial x} \langle T'x' \rangle \end{aligned} \tag{10}$$

Where $\left\langle \kappa_\eta'^2 \right\rangle$, $\left\langle T'^2 \right\rangle$ and $\left\langle x'^2 \right\rangle$ are variance of absorption coefficient κ_η, temperature T and species concentration x, respectively; $\langle T'x' \rangle$ is the covariance of temperature and species concentration.

3.2. From LBL absorption coefficient to LBL transmissivity

Because of the approximately linear relation between absorption coefficient, temperature and species concentration, the absorption coefficients also vary temporally with a Gaussian distribution, which have mean and variance of $\left\langle \kappa_\eta \right\rangle$ and $\left\langle \kappa_\eta'^2 \right\rangle$, respectively. It is known that

$$\begin{aligned} \tau_\eta =& e^{-\int_0^L \kappa_\eta(s)\mathrm{d}s} = e^{-\int_0^L [\langle \kappa_\eta \rangle + \kappa_\eta'(s)]\mathrm{d}s} \\ =& e^{-\langle \kappa_\eta \rangle L} e^{-\int_0^L \kappa_\eta'(s)\mathrm{d}s} \end{aligned} \tag{11}$$

Averaging over Eq. (11) yields

$$\left\langle \tau_\eta \right\rangle = e^{-\langle \kappa_\eta \rangle L} \left\langle e^{-\int_0^L \kappa_\eta'(s)\mathrm{d}s} \right\rangle \tag{12}$$

and the variance of the transmissivity can be written as

$$\left\langle \tau_\eta'^2 \right\rangle = \left\langle \left(\tau_\eta - \left\langle \tau_\eta \right\rangle \right)^2 \right\rangle = \left[e^{-\langle \kappa_\eta \rangle L} \right]^2 \left[\left\langle e^{-2\int_0^L \kappa_\eta'(s)\mathrm{d}s} \right\rangle - \left\langle e^{-\int_0^L \kappa_\eta'(s)\mathrm{d}s} \right\rangle^2 \right] \tag{13}$$

Here we define $\chi_\eta = \int_0^L \kappa_\eta'(s)\mathrm{d}s$ as the turbulence optical thickness, which is a normally distributed random variable with mean $\left\langle \chi_\eta \right\rangle$ and variance $\left\langle \chi_\eta'^2 \right\rangle$. By definition, the positive random variable $e^{-\chi_\eta}$ is log-normally distributed with mean and variance of [49]

$$\langle e^{-\chi_\eta} \rangle = e^{-\langle \chi_\eta \rangle + \frac{1}{2}\langle \chi_\eta'^2 \rangle} \tag{14}$$

$$\mathrm{var}\left(e^{-\chi_\eta}\right) = \langle e^{-\chi_\eta} \rangle^2 \left(e^{\langle \chi_\eta'^2 \rangle} - 1\right) \tag{15}$$

In order to evaluate Eqs. (12) and (13), the mean and variance for the turbulence optical thickness χ_η need to be evaluated first. The mean is

$$\left\langle \chi_\eta \right\rangle = \left\langle \int_0^L \kappa_\eta'(s)\mathrm{d}s \right\rangle = \int_0^L \left\langle \kappa_\eta'(s) \right\rangle \mathrm{d}s = 0 \tag{16}$$

and its variance is

$$\left\langle \chi_\eta'^2 \right\rangle = \left\langle \left[\int_0^L \kappa_\eta'(s)\mathrm{d}s \right]^2 \right\rangle = \int_0^L \int_0^L \left\langle \kappa_\eta'(s_1)\kappa_\eta'(s_2) \right\rangle \mathrm{d}s_1 \mathrm{d}s_2 \tag{17}$$

where $\left\langle \kappa_\eta'(s_1)\kappa_\eta'(s_2) \right\rangle$ is the covariance of absorption coefficients at two different spatial locations s_1 and s_2, and according to Eqs. (8) and (9),

$$\begin{aligned} \left\langle \kappa_\eta'(s_1)\kappa_\eta'(s_2) \right\rangle =& \left\langle \left[\kappa_\eta(s_1) - \left\langle \kappa_\eta(s_1) \right\rangle \right] \left[\kappa_\eta(s_2) - \left\langle \kappa_\eta(s_2) \right\rangle \right] \right\rangle \\ =& \left(\frac{\partial \left\langle \kappa_\eta \right\rangle}{\partial T} \right)^2 \langle T'(s_1)T'(s_2) \rangle + \left(\frac{\partial \left\langle \kappa_\eta \right\rangle}{\partial x} \right)^2 \langle x'(s_1)x'(s_2) \rangle \\ &+ \frac{\partial \left\langle \kappa_\eta \right\rangle}{\partial T} \frac{\partial \left\langle \kappa_\eta \right\rangle}{\partial x} \langle T'(s_1)x'(s_2) \rangle + \frac{\partial \left\langle \kappa_\eta \right\rangle}{\partial x} \frac{\partial \left\langle \kappa_\eta \right\rangle}{\partial T} \langle x'(s_1)T'(s_2) \rangle \end{aligned} \tag{18}$$

For homogeneous turbulence,$\langle x'(s_1)T'(s_2)\rangle = \langle x'(s_2)T'(s_1)\rangle$, so Eq. (18) becomes,

$$\left\langle \kappa'_\eta(s_1)\kappa'_\eta(s_2)\right\rangle = \left(\frac{\partial\left\langle \kappa_\eta\right\rangle}{\partial T}\right)^2 \langle T'(s_1)T'(s_2)\rangle + \left(\frac{\partial\left\langle \kappa_\eta\right\rangle}{\partial x}\right)^2 \langle x'(s_1)x'(s_2)\rangle + 2\frac{\partial\left\langle \kappa_\eta\right\rangle}{\partial T}\frac{\partial\left\langle \kappa_\eta\right\rangle}{\partial x}\langle T'(s_1)x'(s_2)\rangle \tag{19}$$

If the turbulent fields have a spatial correlation function $C_s(r)$, where r is the distance between two arbitrary spatial locations, Eq. (19) can be rewritten as

$$\begin{aligned}\left\langle \kappa'_\eta(s_1)\kappa'_\eta(s_2)\right\rangle = &\left(\frac{\partial\left\langle \kappa_\eta\right\rangle}{\partial T}\right)^2 C_s(|s_1 - s_2|)\left\langle T'^2\right\rangle + \left(\frac{\partial\left\langle \kappa_\eta\right\rangle}{\partial x}\right)^2 C_s(|s_1 - s_2|)\left\langle x'^2\right\rangle \\ &+2\frac{\partial\left\langle \kappa_\eta\right\rangle}{\partial T}\frac{\partial\left\langle \kappa_\eta\right\rangle}{\partial x}C_s(|s_1 - s_2|)\langle T'x'\rangle\end{aligned} \tag{20}$$

let

$$\theta^2 = \frac{1}{L^2}\int_0^L\int_0^L C_s(|s_1 - s_2|)\mathrm{d}s_1\mathrm{d}s_2 \tag{21}$$

then Eq. (17) becomes,

$$\left\langle \chi'^2_\eta\right\rangle = \left\langle \kappa'^2_\eta\right\rangle \theta^2 L^2 \tag{22}$$

Up to here, we have calculated the mean and variance of the turbulence optical thickness χ_η. Applying Eqs. (14) and (15) to Eqs. (12) and (13) yields the mean value for the LBL transmissivity

$$\left\langle \tau_\eta\right\rangle = e^{-\langle\kappa_\eta\rangle L}e^{\frac{1}{2}\langle\kappa'^2_\eta\rangle L^2\theta^2} \tag{23}$$

and variance for LBL transmissivity

$$\left\langle \tau'^2_\eta\right\rangle = \left\langle \tau_\eta\right\rangle^2\left[e^{\langle\kappa'^2_\eta\rangle L^2\theta^2} - 1\right] \tag{24}$$

3.3. Convolution

In the forward calculation, the calculated LBL spectral transmissivity has to be convolved with a pixel response function (PRF) to mimic the resolution of a spectrometer. After transmissivity spectra are convolved with the PRF $\Gamma(\eta)$, they become,

$$\tau_{\eta c} = \int_0^\infty \tau_{\eta_1}\Gamma(\eta - \eta_1)\mathrm{d}\eta_1 \tag{25}$$

After convolution, the time-averaged transmissivity can be rewritten as,

$$\begin{aligned}\langle\tau_c(\eta)\rangle &= \left\langle \int_0^\infty \tau_{\eta_1}\Gamma(\eta - \eta_1)\mathrm{d}\eta_1\right\rangle \\ &= \int_0^\infty \left\langle \tau_{\eta_1}\right\rangle\Gamma(\eta - \eta_1)\mathrm{d}\eta_1\end{aligned} \tag{26}$$

This implies that the convoluted time-averaged lower-resolution transmissivity equals the convolution of the time-averaged LBL transmissivity.

The variance of the convoluted transmissivity is

$$\begin{aligned}\left\langle \tau_{\eta c}'^2 \right\rangle &= \left\langle \left[\int_0^\infty \tau_{\eta_1} \Gamma(\eta - \eta_1) \mathrm{d}\eta_1 - \int_0^\infty \left\langle \tau_{\eta_1} \right\rangle \Gamma(\eta - \eta_1) \mathrm{d}\eta_1 \right]^2 \right\rangle \\ &= \left\langle \left[\int_0^\infty \tau_{\eta_1}' \Gamma(\eta - \eta_1) \mathrm{d}\eta_1 \right]^2 \right\rangle \\ &= \int_0^\infty \int_0^\infty \left\langle \tau_{\eta_1}' \tau_{\eta_2}' \right\rangle \Gamma(\eta - \eta_1) \Gamma(\eta - \eta_2) \mathrm{d}\eta_1 \mathrm{d}\eta_2 \end{aligned} \tag{27}$$

where $\left\langle \tau_{\eta_1}' \tau_{\eta_2}' \right\rangle$ is the covariance of transmissivity τ_η at two arbitrary wavenumber locations η_1 and η_2, where the transmissivity fluctuation is

$$\tau_\eta' = e^{-\langle \kappa_\eta \rangle L} e^{-\int_0^L \kappa_\eta'(s)\mathrm{d}s} - e^{-\langle \kappa_\eta \rangle L} e^{\frac{1}{2}\langle \chi_\eta'^2 \rangle} \tag{28}$$

then $\tau_{\eta_1}' \tau_{\eta_2}'$ can be expressed as

$$\tau_{\eta_1}' \tau_{\eta_2}' = e^{-(\langle \kappa_{\eta_1} \rangle + \langle \kappa_{\eta_2} \rangle) L} \left(e^{-\int_0^L \kappa_{\eta_1}'(s)\mathrm{d}s} - e^{\frac{1}{2}\langle \chi_{\eta_1}'^2 \rangle} \right) \left(e^{-\int_0^L \kappa_{\eta_2}'(s)\mathrm{d}s} - e^{\frac{1}{2}\langle \chi_{\eta_2}'^2 \rangle} \right) \tag{29}$$

Taking the average of Eq. (29) yields the covariance of τ_{η_1} and τ_{η_2},

$$\begin{aligned}\left\langle \tau_{\eta_1}' \tau_{\eta_2}' \right\rangle =& e^{-(\langle \kappa_{\eta_1} \rangle + \langle \kappa_{\eta_2} \rangle) L} \left(\left\langle e^{-\int_0^L (\kappa_{\eta_1}' + \kappa_{\eta_2}')\mathrm{d}s} \right\rangle + e^{\frac{1}{2}\left(\langle \chi_{\eta_1}'^2 \rangle + \langle \chi_{\eta_2}'^2 \rangle\right)} - \left\langle e^{-\int_0^L \kappa_{\eta_1}'(s)\mathrm{d}s} \right\rangle e^{\frac{1}{2}\langle \chi_{\eta_2}'^2 \rangle} - e^{\frac{1}{2}\langle \chi_{\eta_1}'^2 \rangle} \left\langle e^{-\int_0^L \kappa_{\eta_2}'(s)\mathrm{d}s} \right\rangle \right) \\ =& e^{-(\langle \kappa_{\eta_1} \rangle + \langle \kappa_{\eta_2} \rangle) L} \left(\left\langle e^{-\int_0^L (\kappa_{\eta_1}' + \kappa_{\eta_2}')ds} \right\rangle - e^{\frac{1}{2}\left(\langle \chi_{\eta_1}'^2 \rangle + \langle \chi_{\eta_2}'^2 \rangle\right)} \right) \end{aligned} \tag{30}$$

and it is known that

$$\left\langle \int_0^L (\kappa_{\eta_1}' + \kappa_{\eta_2}')\mathrm{d}s \right\rangle = \int_0^L \left\langle (\kappa_{\eta_1}' + \kappa_{\eta_2}') \right\rangle \mathrm{d}s = 0 \tag{31}$$

and

$$\begin{aligned}\left\langle \left[\int_0^L (\kappa_{\eta_1}' + \kappa_{\eta_2}')\mathrm{d}s \right]^2 \right\rangle &= \int_0^L \int_0^L \left\langle \left[\kappa_{\eta_1}'(s_1) + \kappa_{\eta_2}'(s_1) \right] \left[\kappa_{\eta_1}'(s_2) + \kappa_{\eta_2}'(s_2) \right] \right\rangle \mathrm{d}s_1 \mathrm{d}s_2 \\ &= \left\langle \chi_{\eta_1}'^2 \right\rangle + \left\langle \chi_{\eta_2}'^2 \right\rangle + 2 \int_0^L \int_0^L \left\langle \kappa_{\eta_1}'(s_1) \kappa_{\eta_2}'(s_2) \right\rangle \mathrm{d}s_1 \mathrm{d}s_2 \\ &= \left\langle \chi_{\eta_1}'^2 \right\rangle + \left\langle \chi_{\eta_2}'^2 \right\rangle + 2 \left\langle \chi_{\eta_1}' \chi_{\eta_2}' \right\rangle \end{aligned} \tag{32}$$

where $\left\langle \chi_{\eta_1}' \chi_{\eta_2}' \right\rangle = \int_0^L \int_0^L \left\langle \kappa_{\eta_1}'(s_1) \kappa_{\eta_2}'(s_2) \right\rangle \mathrm{d}s_1 \mathrm{d}s_2$ is the covariance of turbulent optical thickness at two arbitrary wavenumber locations η_1 and η_2 and $\left\langle \kappa_{\eta_1}'(s_1) \kappa_{\eta_2}'(s_2) \right\rangle$ is the covariance of absorption coefficients at two arbitrary wavenumber locations η_1 and η_2 as well as at two arbitrary spatial locations s_1 and s_2, which can be calculated from

$$\begin{aligned}\left\langle \kappa_{\eta_1}'(s_1) \kappa_{\eta_2}'(s_2) \right\rangle =& \frac{\partial \left\langle \kappa_{\eta_1} \right\rangle}{\partial T} \frac{\partial \left\langle \kappa_{\eta_2} \right\rangle}{\partial T} \left\langle T'(s_1) T'(s_2) \right\rangle + \frac{\partial \left\langle \kappa_{\eta_1} \right\rangle}{\partial x} \frac{\partial \left\langle \kappa_{\eta_2} \right\rangle}{\partial x} \left\langle x'(s_1) x'(s_2) \right\rangle \\ &+ \left(\frac{\partial \left\langle \kappa_{\eta_1} \right\rangle}{\partial T} \frac{\partial \left\langle \kappa_{\eta_2} \right\rangle}{\partial x} + \frac{\partial \left\langle \kappa_{\eta_1} \right\rangle}{\partial x} \frac{\partial \left\langle \kappa_{\eta_2} \right\rangle}{\partial T} \right) \left\langle T'(s_1) x'(s_2) \right\rangle \end{aligned} \tag{33}$$

For turbulent fields with a spatial correlation function $C_s(r)$, the covariance of turbulent optical thickness

$\left\langle \chi'_{\eta_1}\chi'_{\eta_2}\right\rangle$ can be calculated as

$$\begin{aligned}\left\langle \chi'_{\eta_1}\chi'_{\eta_2}\right\rangle =& \int_0^L\int_0^L \left\langle \kappa'_{\eta_1}(s_1)\kappa'_{\eta_2}(s_2)\right\rangle \mathrm{d}s_1\mathrm{d}s_2\\ =&\frac{\partial\left\langle\kappa_{\eta_1}\right\rangle}{\partial T}\frac{\partial\left\langle\kappa_{\eta_2}\right\rangle}{\partial T}\left\langle T'^2\right\rangle\int_0^L\int_0^L C_s(|s_1-s_2|)\mathrm{d}s_1\mathrm{d}s_2+\frac{\partial\left\langle\kappa_{\eta_1}\right\rangle}{\partial x}\frac{\partial\left\langle\kappa_{\eta_2}\right\rangle}{\partial x}\left\langle x'^2\right\rangle\int_0^L\int_0^L C_s(|s_1-s_2|)\mathrm{d}s_1\mathrm{d}s_2\\ &+\left(\frac{\partial\left\langle\kappa_{\eta_1}\right\rangle}{\partial T}\frac{\partial\left\langle\kappa_{\eta_2}\right\rangle}{\partial x}+\frac{\partial\left\langle\kappa_{\eta_1}\right\rangle}{\partial x}\frac{\partial\left\langle\kappa_{\eta_2}\right\rangle}{\partial T}\right)\langle T'x'\rangle\int_0^L\int_0^L C_s(|s_1-s_2|)\mathrm{d}s_1\mathrm{d}s_2\\ =&\theta^2L^2\left[\frac{\partial\left\langle\kappa_{\eta_1}\right\rangle}{\partial T}\frac{\partial\left\langle\kappa_{\eta_2}\right\rangle}{\partial T}\left\langle T'^2\right\rangle+\frac{\partial\left\langle\kappa_{\eta_1}\right\rangle}{\partial x}\frac{\partial\left\langle\kappa_{\eta_2}\right\rangle}{\partial x}\left\langle x'^2\right\rangle+\left(\frac{\partial\left\langle\kappa_{\eta_1}\right\rangle}{\partial T}\frac{\partial\left\langle\kappa_{\eta_2}\right\rangle}{\partial x}+\frac{\partial\left\langle\kappa_{\eta_1}\right\rangle}{\partial x}\frac{\partial\left\langle\kappa_{\eta_2}\right\rangle}{\partial T}\right)\langle T'x'\rangle\right] \quad (34)\end{aligned}$$

So Eq. (30) reduces to

$$\begin{aligned}\left\langle \tau'_{\eta_1}\tau'_{\eta_2}\right\rangle =&e^{-(\langle\kappa_{\eta_1}\rangle+\langle\kappa_{\eta_2}\rangle)L}e^{\frac{1}{2}\left\langle\chi'^2_{\eta_1}\right\rangle+\frac{1}{2}\left\langle\chi'^2_{\eta_2}\right\rangle}\left(e^{\left\langle\chi'_{\eta_1}\chi'_{\eta_2}\right\rangle}-1\right)\\ =&\left\langle\tau_{\eta_1}\right\rangle\left\langle\tau_{\eta_2}\right\rangle\left(e^{\left\langle\chi'_{\eta_1}\chi'_{\eta_2}\right\rangle}-1\right)\\ \approx&\left\langle\tau_{\eta_1}\right\rangle\left\langle\tau_{\eta_2}\right\rangle\left\langle\chi'_{\eta_1}\chi'_{\eta_2}\right\rangle \quad (35)\end{aligned}$$

and Eq. (27) becomes

$$\left\langle\tau'^2_{\eta c}\right\rangle=\int_0^\infty\int_0^\infty\left(\left\langle\tau_{\eta_1}\right\rangle\left\langle\tau_{\eta_2}\right\rangle\left\langle\chi'_{\eta_1}\chi'_{\eta_2}\right\rangle\right)\Gamma(\eta-\eta_1)\Gamma(\eta-\eta_2)\mathrm{d}\eta_1\mathrm{d}\eta_2 \quad (36)$$

4. Inverse calculation

The present study is limited to homogeneous turbulent fields of a N_2+CO_2, N_2+H_2O or N_2+CO mixtures and, therefore, the parameters that need to be determined are the time-averaged temperature $\langle T\rangle$ and concentration $\langle x\rangle$, the variance of temperature $\left\langle T'^2\right\rangle$ and concentration $\left\langle x'^2\right\rangle$, and the covariance of temperature and concentration $\langle T'x'\rangle$. Usually, the turbulence length scale Λ is an unknown parameter, so it also need to be determined.

Assuming time-averaged transmissivity and its variance can be optically measured at a relatively low resolution, generally the equations we need to solve to obtain all the parameters are

$$\left\langle\tau_{\eta c}\right\rangle=f_\eta\left(\langle T\rangle,\langle x\rangle,\left\langle T'^2\right\rangle,\left\langle x'^2\right\rangle,\langle T'x'\rangle,\Lambda\right) \quad (37)$$

or

$$\left\langle\tau'^2_{\eta c}\right\rangle=g_\eta\left(\langle T\rangle,\langle x\rangle,\left\langle T'^2\right\rangle,\left\langle x'^2\right\rangle,\langle T'x'\rangle,\Lambda\right) \quad (38)$$

where the nonlinear functions f_η and g_η can be determined with Eqs. (26) and (27), respectively. In principle, either of Eqs. (37) and (38) can be used to solve all the parameters if one measures the time-averaged transmissivity or the variance of transmissivity with a certain spectral resolution, obtaining enough discrete values at different wavenumbers. However, these two equations show different sensitivity to different parameters, as indicated in Eqs. (23) and (24). In Eq. (23), the term $e^{\frac{1}{2}\left\langle\kappa'^2_\eta\right\rangle L^2\theta^2}$ gives the effect of turbulent fluctuations on transmissivity of the gaseous medium. It is easy to demonstrate this term is larger than unity, which means turbulent fluctuations increase transmissivity. But if the optical thickness of the gas medium based on the turbulent integral length scale ($\kappa_\eta\Lambda$) is small, this term is always close to unity, i.e., time-averaged transmissivity is not sensitive to the intensity of turbulence fluctuations. By contrast, as shown in Eq. (24), turbulent fluctuations always have significant effects on the fluctuation of transmissivities. Deducing $\langle T\rangle$, $\langle x\rangle$, $\left\langle T'^2\right\rangle$, $\left\langle x'^2\right\rangle$, $\langle T'x'\rangle$

and Λ from Eqs. (37) or (38) requires deconvolution and makes these problems ill-posed and, therefore these equations cannot be inverted directly to obtain all the parameters. Inverse procedures are required to solve them numerically. In this study, time-averaged temperature $\langle T \rangle$ and concentration $\langle x \rangle$ are solved by minimizing an objective function F_1, which represents the difference between the predicted and measured time-averaged transmissivity, i.e.,

$$F_1(\vec{a}_1) = \sum_{i=1}^{I} (\langle \tau_{ic} \rangle - f_i)^2 \tag{39}$$

where i denotes discrete wavenumber. The variance of temperature $\left\langle T'^2 \right\rangle$ and concentration $\left\langle x'^2 \right\rangle$, the covariance of temperature and concentration $\langle T'x' \rangle$ and the turbulence length scale Λ are solved by minimizing an objective function F_2, which represents the difference between the predicted and measured variance of transmissivity, i.e.,

$$F_2(\vec{a}_2) = \sum_{i=1}^{I} \left(\left\langle \tau_{ic}'^2 \right\rangle - g_i \right)^2 \tag{40}$$

Here we separate all unknown parameters into two parameter vectors, where $\vec{a}_1 = (\langle T \rangle, \langle x \rangle)^T$ is solved from Eq. (39) and $\vec{a}_2 = \left(\left\langle T'^2 \right\rangle, \left\langle x'^2 \right\rangle, \langle T'x' \rangle, \Lambda \right)^T$ is solved from Eq. (40). The goal of inverse calculations is to minimize these two functions by properly guessing the parameter vectors until the best matches between the measured spectra and predicted spectra data are achieved. In our previous study [11, 12], the Levenberg-Marquardt optimization method was applied to retrieve temperatures and species concentrations for laminar gaseous media. We found the Levenberg-Marquardt optimization method to be relatively reliable, more accurate and requiring less computational effort than several other methods tested. Therefore, the Levenberg-Marquardt is also employed in the present study. In this method, the parameter vector $\vec{a}$ is gradually increased by a small value $\vec{\delta a}$,

$$\vec{a}_{new} = \vec{a}_{old} + \delta\vec{a} \tag{41}$$

with

$$\delta\vec{a} = -H'^{-1}B \tag{42}$$

and the vector $B = \nabla F(\vec{a})$ is the gradient vector of the objective function F with respect to $\vec{a}$, and H' is a matrix with elements

$$h'_{ij} = \begin{cases} (1+\lambda)h_{ij} & i = j \\ h_{ij} & i \neq j \end{cases} \tag{43}$$

where the h_{ij} are the elements of the Hessian matrix $H = \nabla^2 F(\vec{a})$.

The nonnegative scaling factor, λ, is adjusted at each iteration. If reduction of the objective function is rapid, a smaller value can be used, whereas if an iteration gives insufficient reduction, λ can be increased. If $\delta\vec{a}$ gets sufficiently small, the iteration will stop and the parameter vector $\vec{a}$ will be obtained. The Levenberg-Marquardt method increases the value of each diagonal term of the ill-conditioned Hessian matrix H (regularization), to mitigate the ill-posedness of the problem. Details for the computational algorithm using the Levenberg-Marquardt method can be found in [11, 12, 50]. the procedure for retrieving all the parameters is summarized as follows

1. Assume starting points for $\vec{a}_1$ and $\vec{a}_2$.
2. Fix $\vec{a}_2$ and apply the Levenberg-Marquardt method to Eq. (39) to update $\vec{a}_1$.
3. With the updated $\vec{a}_1$, apply the Levenberg-Marquardt method again to Eq. (40) to update $\vec{a}_2$.
4. With the updated $\vec{a}_2$, go back to 2 and update $\vec{a}_1$ again.
5. Stop iteration when the changes of $\vec{a}_1$ and $\vec{a}_2$ become sufficiently small

5. Results and discussion

Instantaneous transmissvities $\tau_{\eta c}$ are calculated from Eq. (6) for the instantaneous temperature and species concentration fields for CO_2, H_2O and CO. Stochastic analysis was conducted to calculate the time-averaged

transmissivity and their rms spectra, which are denoted as "actual" spectra and were used to retrieve temperature $\langle T \rangle$, concentration $\langle x \rangle$ and their variance $\left\langle T'^2 \right\rangle$, $\left\langle x'^2 \right\rangle$ and $\langle T'x' \rangle$ for the three species from the inverse calculation model. On the other hand, these mean and rms values can also be directly calculated from the turbulence fields by conducting a stochastic analysis and the results are shown in Table 1, denoted as "actual values", which are used as the benchmark for the retrieved values from inverse calculations.

The "actual" time-averaged transmissivity and their rms spectra for CO_2, H_2O and CO were used to retrieve temperature, concentration, their rms values and turbulent length scale. The performance of different spectral bands for inverse calculation was investigated, and the retrieved results are shown in Table 1. *Actual* transmissivity and their rms spectra are compared with the spectra calculated with the *retrieved* parameter values in Table 1 from Eqs. (26) and (27) and also compared with the spectra calculated from *forward* calculations with the actual parameter values in Table 1 from Eqs. (26) and (27). All comparisons are shown in Figs. 3, 4 and 5.

Table 1: Inverse calculation results for retrieving temperatures, species concentrations, their rms values and turbulent length scales from time-averaged transmissivity spectra and their rms spectra

retrieved parameters		$\langle T \rangle$ (K)	$\langle x \rangle$	$\sqrt{\langle T'^2 \rangle}$ (K)	$\sqrt{\langle x'^2 \rangle}$	$\langle T'x' \rangle$ (K)	Λ/L
actual values		1495	0.0997	150.8	0.0101	1.23	0.100
CO_2 4.3 μm	retrieved	1524	0.1017	145.2	0.0125	1.24	0.092
(1900 to 2500 cm^{-1})	error(%)	1.95	2.04	−3.73	24.21	0.89	−7.93
CO_2 2.7 μm	retrieved	1498	0.0995	149.5	0.0101	1.23	0.099
(3300 to 3800 cm^{-1})	error(%)	0.21	−0.19	−0.91	0.64	−0.12	−0.78
H_2O 2.7 μm	retrieved	1490	0.0994	151.0	0.0098	1.23	0.102
(3200 to 4200 cm^{-1})	error(%)	−0.34	−0.26	0.13	−3.04	−0.12	1.58
H_2O 1.8 μm	retrieved	1491	0.0994	149.6	0.0101	1.24	0.099
(4800 to 5800 cm^{-1})	error(%)	−0.25	−0.24	−0.79	0.04	0.74	−1.37
CO 4.7 μm	retrieved	1496	0.1006	149.5	0.01	1.22	0.099
(1800 to 3900 cm^{-1})	error(%)	0.03	0.95	−0.87	−0.25	−0.79	−0.75
CO 2.3 μm	retrieved	1497	0.1	149.8	0.0095	1.22	0.100
(3900 to 4400 cm^{-1})	error(%)	0.15	0.36	−0.69	−5.43	−0.86	0.07

Two CO_2 spectral bands at 4.3 and 2.7 μm were tested. The retrieved parameters are shown in Table 1. Large errors occur when retrieving rms values for CO_2 concentration from the 4.3 μm band and the retrieved turbulent length scale also has a relatively large discrepancy from the actual value. For the CO_2 2.7 μm band all retrieved results are very accurate: differences from actual parameter values are less than 1%. Figure 3 shows the comparison of retrieved transmissivity and their rms spectra with the "actual" spectra and forward spectra for the CO_2 4.3 and 2.7 μm bands. It appears that the forward calculated transmissivity and the rms spectra are overestimated at lower wavenumbers for the CO_2 4.3 μm band compared with the "actual" spectra. In the forward calculation model, we invoke the assumption that the spectral absorption coefficient is only a linear function over the temperature range of $\langle T \rangle \pm T'_{max}$ and species concentration range of $\langle x \rangle \pm x'_{max}$, as given by Eq. (8). The linear assumption for absorption coefficients with concentration is valid due to weak self-broadening effects of CO_2. However, for the the CO_2 4.3 μm band, the spectral absorption coefficient may be slightly nonlinear over the temperature range 1500±150 K. Comparing to the CO_2 2.7 μm band, the CO_2 4.3 μm band is so strong that slightly nonlinearity may cause large discrepancies for larger optical thickness ($\langle \kappa_\eta \rangle L$). This is easy to demonstrate from Eqs. (23) and (24).

Two H_2O spectral bands at 2.7 μm and 1.8 μm and two CO spectral bands at 4.7 μm and 1.8 μm were also tested using transmissivity data synthesized from the turbulence fields. Table 1 shows the inverse results and Figs 4 and 5 show the comparison of retrieved transmissivity and their rms spectra with the "actual" spectra and spectra calculated from forward calculation model. For these H_2O and CO transmissivity spectral bands, retrieved and forward spectra perfectly overlap with the "actual" spectra. Although "actual" and forward rms spectra show discrepancies with the "actual" rms spectra at smaller rms values, the spectral peaks and most part of the "actual" rms spectra bands are well captured by the retrieved and forward rms spectra. This shows

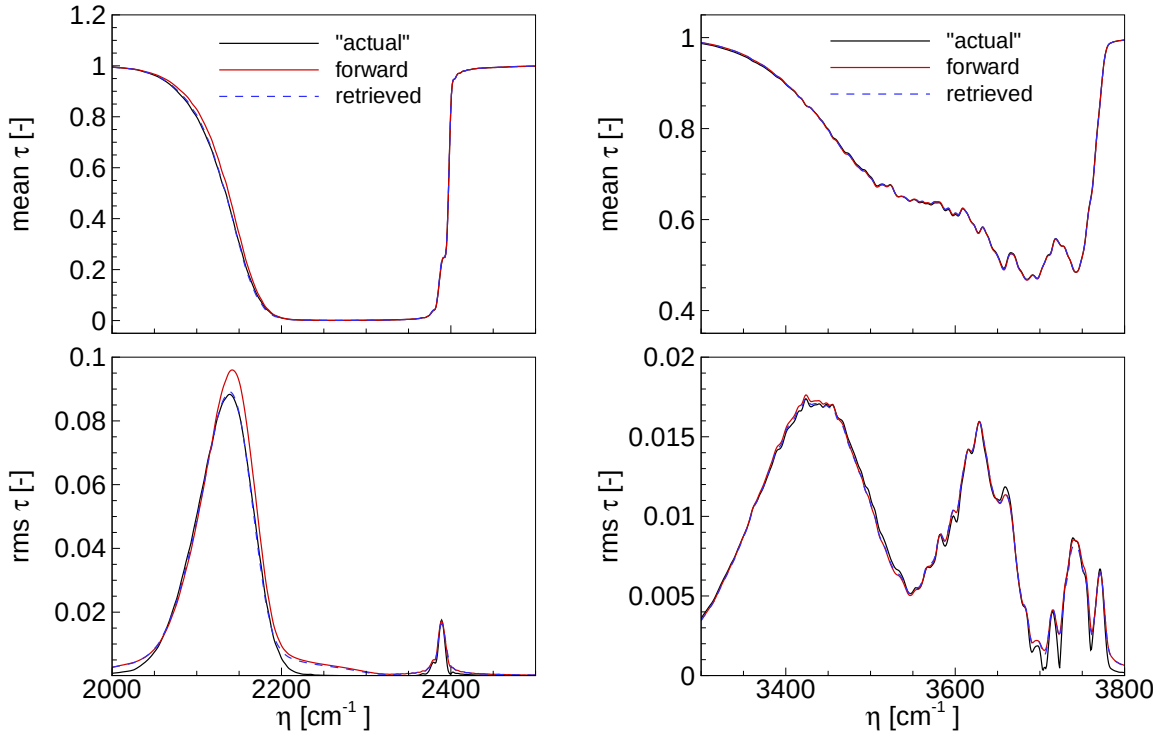

Figure 3: Comparison of retrieved transmissivity and its rms spectra with the "actual" spectra and forward spectra calculated by the actual turbulent scalars for the CO_2 4.3 μm and 2.7 μm bands

that the forward calculations for predicting lower-resolution time-averaged transmissivities and their rms values are accurate enough and the resulting inverse radiation model provides a reliable tool for retrieving mean temperature, concentration, their rms values and turbulent length scale from synthetic turbulent transmissivity measurements.

All the previous test cases are for perfectly correlated temperature and species concentration fields, i.e., $u_T = u_x$ as in Eqs. (4a) and (4a). Although experiments show there are strong correlations between temperature and species concentration for flame [52], for our proposed method, there is no pre-assumption for the correlation between temperature and species concentration. Time-averaged temperature and species concentration are retrieved simultaneously and independently. Table 2 shows the results for non-correlated temperature and species concentration fields (other conditions remain the same). Except large errors occur when retrieving rms values for species concentration from the strong CO_2 4.3 μm band in this case, acceptable results are obtained from the CO_2 2.7 μm band as well as from other bands of the other two species.

Although "actual" spectra can be well captured by "forward" spectra. There are three sources for the small discrepancies between the "actual" and the "forward" spectra:

1. Statistical uncertainty
   "Actual" transmissivity and its variance were obtained by conducting stochastic calculations using the instantaneous transmissivity. Due to the finite number of time realizations of turbulent scalars, there are statistical uncertainties associated with them.
2. Linear assumption for absorption coefficient with temperature and concentration
   The absorption coefficient was linearized locally with temperature and gas concentration. This is not a very good approximation for a spectral interval where the absorption coefficient is very large, for example, the CO_2 4.3 μm band.
3. Optically thin approximation
   To calculate the variance of transmissivity, there is an approximation for Eq. (35). This approximation

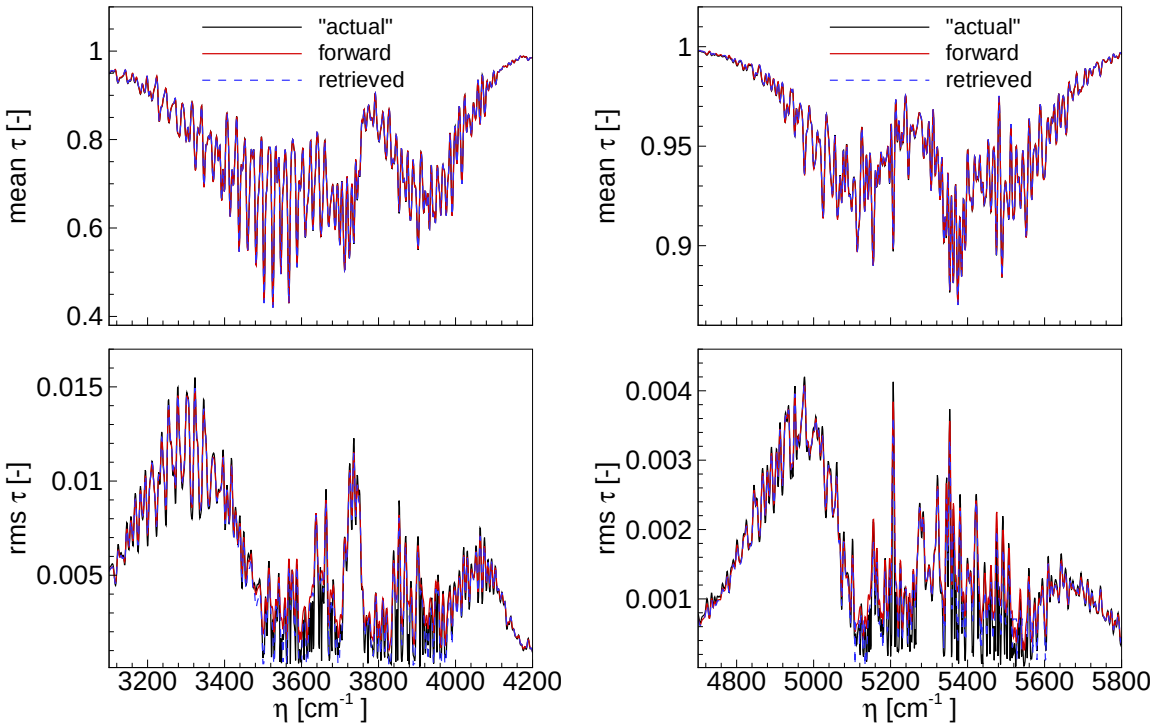

Figure 4: Comparison of retrieved transmissivity and its rms spectra with the "actual" spectra and forward spectra calculated by the actual turbulent scalars for the H_2O 2.7 μm and 1.8 μm bands

Table 2: Inverse calculation results for retrieving temperatures, species concentrations, their rms values and turbulent length scales from time-averaged transmissivity spectra and their rms spectra for non-correlated temperature and species concentration fields.

retrieved parameters		$\langle T \rangle$ (K)	$\langle x \rangle$	$\sqrt{\langle T'^2 \rangle}$ (K)	$\sqrt{\langle x'^2 \rangle}$	$\langle T'x' \rangle$ (K)	Λ/L
actual values		1495	0.1001	150.8	0.0101	0	0.100
CO_2 4.3 μm	retrieved	1510	0.1021	143.8	0.0151	0.08	0.091
(1900 to 2500 cm^{-1})	error(%)	1.00	2.06	−4.65	49.7	–	−8.70
CO_2 2.7 μm	retrieved	1483	0.0999	150.6	0.01	−0.05	0.101
(3300 to 3800 cm^{-1})	error(%)	−0.81	−0.17	−0.16	−0.99	–	1.08
H_2O 2.7 μm	retrieved	1475	0.0998	154.6	0.009	-0.05	0.107
(3200 to 4200 cm^{-1})	error(%)	−1.37	−0.24	2.48	−11.03	–	6.61
H_2O 1.8 μm	retrieved	1476	0.0998	154.1	0.0088	-0.05	0.106
(4800 to 5800 cm^{-1})	error(%)	−1.28	−0.24	2.16	−12.72	–	5.94
CO 4.7 μm	retrieved	1480	0.101	152.6	0.0094	-0.15	0.104
(1800 to 2400 cm^{-1})	error(%)	−1.00	0.99	1.18	−6.96	–	4.18
CO 2.3 μm	retrieved	1482	0.1004	151.6	0.0094	-0.13	0.102
(3900 to 4400 cm^{-1})	error(%)	−0.88	0.38	0.48	−6.16	–	1.85

is only valid if the covariance of turbulent optical thickness is small. For an optically thick spectral interval, the covariance of turbulent optical thickness can be very large. However, according to Eq. (35), at optically thick parts of the spectrum, transmissivities approach zero and make this part of the rms spectrum approach zero as well, making this part of the spectrum less important.

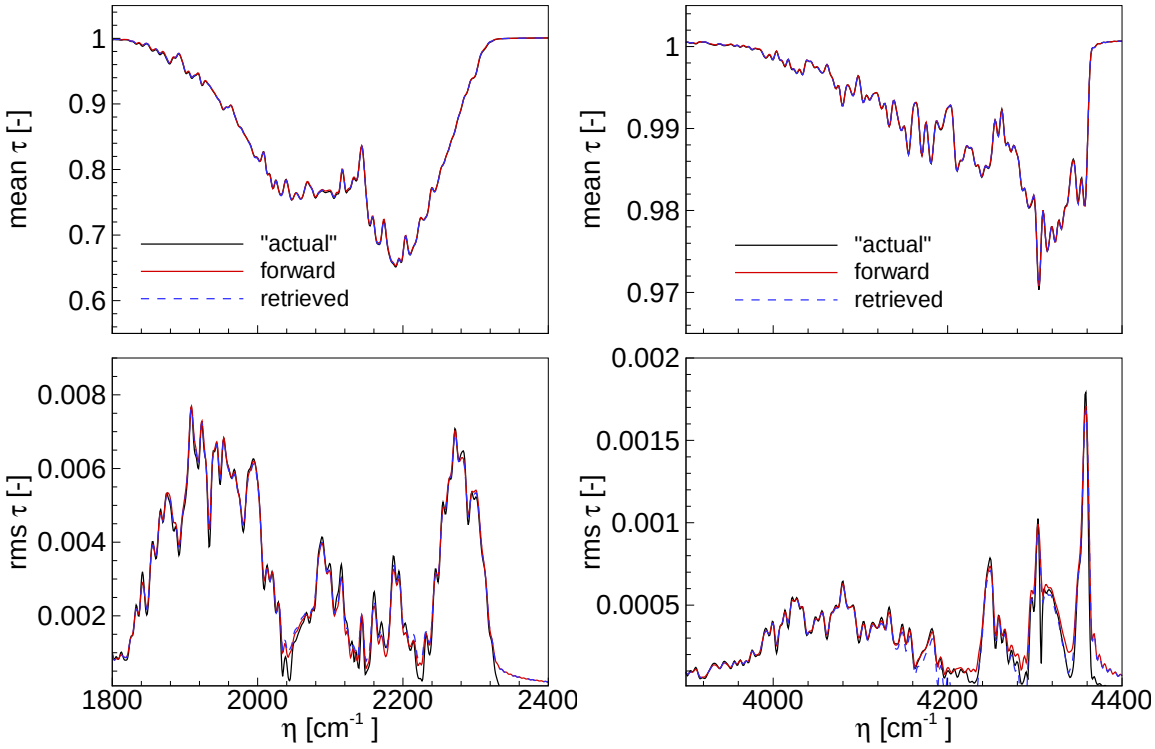

Figure 5: Comparison of retrieved transmissivity and its rms spectra with the "actual" spectra and forward spectra calculated by the actual turbulent scalars for the CO 4.7 μm and 2.3 μm bands

6. Conclusions

An inverse radiation model was developed to reconstruct time-averaged temperature, species concentration, their rms values and turbulence length scale from time-averaged transmissivity and its rms spectra for homogeneous gas media. Synthetic turbulence fields were created for temperatures and species concentrations and synthetic turbulent transmissivity spectra were created for CO_2, H_2O and CO based on the created turbulence fields. Statistical parameters from the turbulence fields and time-averaged transmissivity and rms transmissivity spectra calculated from instantaneous turbulent transmissivity spectra were used to validate the inverse radiation model. Results show that, by considering interaction between turbulence and radiation, time-averaged temperature, concentration, their rms values and turbulent length scale can be accurately retrieved from synthetic turbulent transmissivity measurements.

Acknowledgment

The authors gratefully acknowledge the support from National Science Foundation Grant No. CBET-0966627 and the help from Dr. Soufiani for generating the turbulence fields.

References

[1] R. J. Anderson, P. R. Griffiths, Determination of rotational temperatures of diatomic molecules from absorption spectra measured at moderate resolution, J Quant Spectrosc Radiat Transf 17 (1977) 393–401.

[2] L. A. Gross, P. R. Griffiths, Temperature estimation of carbon dioxide by infrared absorption spectrometry at medium resolution, J Quant Spectrosc Radiat Transf 39 (2) (1988) 131–138.

[3] P. J. Hommert, R. Viskanta, A. M. Mellor, Flame temperature measurements by spectral remote sensing, Combust Flame 30 (1977) 295–308.

[4] D. R. Buchele, Computer program for calculation of a gas temperature profile by infrared emission: Absorption spectroscopy, NASA-TM-73848.

[5] P. R. Solomon, P. E. Best, R. M. Carangelo, J. R. Markham, P.-L. Chien, R. J. Santoro, H. G. Semerjian, Ft-ir emission/transmission spectroscopy for in situ combustion diagnostics, Proc Comb Inst 21 (1987) 1763–1771.

[6] P. E. Best, P. L. Chien, R. M. Carangelo, P. R. Solomon, M. Danchak, I. Ilovici, Tomographic reconstruction of ft-ir emission and transmission spectra in a sooting laminar diffusion flame: Species concentrations and temperatures, Combust Flame 85 (1991) 309–314.

[7] S.-W. Woo, T.-H. Song, Measurement of gas temperature profile using spectral intensity from co_2 4.3 μm band, International journal of thermal sciences 41 (9) (2002) 883–890.

[8] H. K. Kim, T.-H. Song, Characteristics of srs inversion for measurement of temperature and co_2 concentration profile of a combustion gas layer, J Quant Spectrosc Radiat Transf 86 (2) (2004) 181–199.

[9] H. K. Kim, T.-H. Song, Determination of the gas temperature profile in a large-scale furnace using a fast/efficient inversion scheme for the SRS technique, J Quant Spectrosc Radiat Transf 93 (2005) 369–381.

[10] T.-H. Song, Spectral remote sensing for furnaces and flames, Heat Transfer Engineering 29 (4) (2008) 417–428.

[11] T. Ren, M. F. Modest, Temperature profile inversion from CO_2 spectral intensities through levenberg-marquardt optimization and tikhonov regularization, in: Paper No.1896725, 11th AIAA/ASME Joint Thermophysics and Heat Transfer Conference, Atlanta, GA, 2014.

[12] T. Ren, M. F. Modest, An inverse radiation model for optical determination of temperature and species concentration: development and validation, J Quant Spectrosc Radiat Transf 151 (0) (2015) 198–209.

[13] A. A. Townsend, The effects of radiative transfer on turbulent flow of a stratified fluid, J Fluid Mech 4 (1958) 361–375.

[14] T.-H. Song, R. Viskanta, Interaction of radiation with turbulence: Application to a combustion system, J Thermoph Heat Transfer 1 (1987) 56–62.

[15] A. Soufiani, P. Mignon, J. Taine, Radiation–turbulence interaction in channel flows of infrared active gases, in: Proceedings of the International Heat Transfer Conference, Vol. 6, ASME, 1990, pp. 403–408.

[16] R. J. Hall, A. Vranos, Efficient calculations of gas radiation from turbulent flames, Intl J Heat Mass Transfer 37 (17) (1994) 2745–2750.

[17] S. Tieszen, On the fluid mechanics of fires, Ann. Rev. Fluid Mech. 33 (2001) 67–92.

[18] S. M. Jeng, M. C. Lai, G. M. Faeth, Nonluminous radiation in turbulent buoyant axisymmetric flames, Combust Sci Technol 40 (1984) 41–53.

[19] J. P. Gore, G. M. Faeth, Structure and spectral radiation properties of turbulent ethylene/air diffusion flames, in: Proceedings of the Twenty-First Symposium (International) on Combustion, 1986, pp. 1521–1531.

[20] J. P. Gore, S. M. Jeng, G. M. Faeth, Spectral and total radiation properties of turbulent carbon monoxide/air diffusion flames, AIAA J 25 (2) (1987) 339–345.

[21] J. P. Gore, S. M. Jeng, G. M. Faeth, Spectral and total radiation properties of turbulent hydrogen/air diffusion flames, ASME J Heat Transfer 109 (1987) 165–171.

[22] M. E. Kounalakis, J. P. Gore, G. M. Faeth, Turbulence/radiation interactions in nonpremixed hydrogen/air flames, in: Twenty-Second Symposium (International) on Combustion, The Combustion Institute, 1988, pp. 1281–1290.

[23] M. E. Kounalakis, J. P. Gore, G. M. Faeth, Mean and fluctuating radiation properties of nonpremixed turbulent carbon monoxide/air flames, ASME J Heat Transfer 111 (1989) 1021–1030.

[24] Y. R. Sivathanu, M. E. Kounalakis, G. M. Faeth, Soot and continuous radiation statistics of luminous turbulent diffusion flames, in: Twenty-Third Symposium (International) on Combustion, The Combustion Institute, 1990, pp. 1543–1550.

[25] M. Klassen, Y. R. Sivathanu, J. P. Gore, Simultaneous emission absorption-measurements in toluene-fueled pool flames – mean and rms properties, Combust Flame 90 (1992) 34–44.

[26] Y. R. Sivathanu, J. P. Gore, Transient structure and radiation properties of strongly radiating buoyant flames, ASME J Heat Transfer 114 (1992) 659–665.

[27] Y. Zheng, R. S. Barlow, J. P. Gore, Spectral radiation properties of partially premixed turbulent flames, ASME J Heat Transfer 125 (2003) 1065–1073.

[28] Y. Zheng, R. S. Barlow, J. P. Gore, Measurements and calculations of spectral radiation intensities for turbulent non-premixed and partially premixed flames, ASME J Heat Transfer 125 (2003) 678–686.

[29] Y. Zheng, J. P. Gore, Measurements and inverse calculations of spectral radiation intensities of a turbulent ethylene/air jet flame, in: Thirtieth Symposium (International) on Combustion, The Combustion Institute, 2005, pp. 727–734.

[30] D. L. Blunck, M. E. H. C. L. Merkle, J. P. Gore, Influence of turbulent fluctuations on the radiation intensity emitted from exhaust plumes, J Thermoph Heat Transfer 26 (4) (2012) 581–589.

[31] D. Blunck, M. Harvazinski, B. Rankin, C. Merkle, J. Gore, Turbulent radiation statistics of exhaust plumes exiting from a subsonic axisymmetric nozzle, J Thermoph Heat Transfer 26 (2) (2012) 286–293.

[32] S. Mazumder, M. F. Modest, PDF modeling of turbulence radiation interactions, in: 1997 National Heat Transfer Conference, Baltimore, MD, ASME, 1997.

[33] S. Mazumder, M. F. Modest, Turbulence–radiation interactions in nonreactive flow of combustion gases, ASME J Heat Transfer 121 (1999) 726–729.

[34] G. Li, M. F. Modest, A PDF method to capture sharp gradients in turbulent heat transfer, in: Proceedings of the 2000 National Heat Transfer Conference, ASME, Pittsburgh, PA, 2000.

[35] G. Li, M. F. Modest, Application of composition PDF methods in the investigation of turbulence–radiation interactions, J Quant Spectrosc Radiat Transf 73 (2002) 461–472.

[36] A. Gupta, D. C. Haworth, M. F. Modest, Turbulence-radiation interactions in large-eddy simulations of luminous and nonluminous nonpremixed flames, Proc Comb Inst 34 (2013) 1281–1288.

[37] P. J. Coelho, Numerical simulation of the interaction between turbulence and radiation in reactive flows, Progr Energy Combust Sci 33 (4) (2007) 311–383.

[38] V. P. Kabashinikov, G. I. Myasnikova, Thermal radiation in turbulent flows—temperature and concentration fluctuations, Heat Transfer-Soviet Research 17 (6) (1985) 116–125.

[39] J. Y. Ko, H. K. Kim, T.-H. Song, Inversion of combustion gas temperature/concentration profile with radiation/turbulence interaction using SRS, J Quant Spectrosc Radiat Transf 110 (13) (2009) 1199–1206.

[40] P. Foster, Relation of time-mean transmission of turbulent flames to optical depth, Journal of the Institute of Fuel 42 (340) (1969) 179.

[41] L. S. Rothman, I. E. Gordon, R. J. Barber, H. Dothe, R. R. Gamache, A. Goldman, V. I. Perevalov, S. A. Tashkun, J. Tennyson, HITEMP, the high-temperature molecular spectroscopic database, J Quant Spectrosc Radiat Transf 111 (15) (2010) 2139–2150.

[42] M. F. Modest, S. P. Bharadwaj, High-resolution, high-temperature transmissivity measurements and correlations for carbon dioxide–nitrogen mixtures, J Quant Spectrosc Radiat Transf 73 (2–5) (2002) 329–338.

[43] S. P. Bharadwaj, M. F. Modest, Medium resolution transmission measurements of CO_2 at high temperature – an update, J Quant Spectrosc Radiat Transf 103 (2007) 146–155.

[44] V. Evseev, A. Fateev, S. Clausen, High-resolution transmission measurements of CO_2 at high temperatures for industrial applications, J Quant Spectrosc Radiat Transf 113 (2012) 2222–2233.

[45] S. P. Bharadwaj, M. F. Modest, R. J. Riazzi, Medium resolution transmission measurements of water vapor at high temperature, ASME J Heat Transfer 128 (2006) 374–381.

[46] A. Fateev, S. Clausen, On-line non-contact gas analysis, Danmarks Tekniske Universitet, Risø National-laboratoriet for Bæredygtig Energi, 2008.

[47] F. Kritzstein, A. Soufiani, Infrared gas radiation from a homogeneously turbulent medium, Intl J Heat Mass Transfer 36 (7) (1993) 1749–1762.

[48] L. Soucasse, P. Rivière, A. Soufiani, Subgrid-scale model for radiative transfer in turbulent participating media, J Comp Phys 257 (2014) 442–459.

[49] S. B. Pope, Turbulent Flows, Cambridge University Press, Cambridge, 2000.

[50] W. H. Press, S. A. Teukolsky, W. T. Vetterling, B. P. Flannery, Numerical Recipies in FORTRAN – The Art of Scientific Computing, 2nd Edition, Cambridge University Press, Cambridge, 1992.

[51] C. B. da Silva, I. Malico, P. J. Coelho, Radiation statistics in homogeneous isotropic turbulence, New Journal of Physics 11 (9) (2009) 093001.

[52] R. S. Barlow, International workshop on measurement and computation of turbulent nonpremixed flames (TNF), website: http://www.sandia.gov/TNF/abstract.html.